fractal and fractional

MDPI

Article

Partially Penetrated Well Solution of Fractal Single-Porosity Naturally Fractured Reservoirs

Ricardo Posadas-Mondragón [1] and Rodolfo G. Camacho-Velázquez [2,*]

[1] Pemex Exploración y Producción, 11311 Mexico City, Mexico; ricardo.posadas@pemex.com
[2] Engineering Faculty, National University of Mexico, UNAM, Circuito Exterior, Ciudad Universitaria, 04510 Mexico City, Mexico
* Correspondence: camachovrodolfo@gmail.com; Tel.: +52-1-55-4055-6329

Received: 6 April 2019; Accepted: 18 April 2019; Published: 24 April 2019

Abstract: In the oil industry, many reservoirs produce from partially penetrated wells, either to postpone the arrival of undesirable fluids or to avoid problems during drilling operations. The majority of these reservoirs are heterogeneous and anisotropic, such as naturally fractured reservoirs. The analysis of pressure-transient tests is a very useful method to dynamically characterize both the heterogeneity and anisotropy existing in the reservoir. In this paper, a new analytical solution for a partially penetrated well based on a fractal approach to capture the distribution and connectivity of the fracture network is presented. This solution represents the complexity of the flow lines better than the traditional Euclidean flow models for single-porosity fractured reservoirs, i.e., for a tight matrix. The proposed solution takes into consideration the variations in fracture density throughout the reservoir, which have a direct influence on the porosity, permeability, and the size distribution of the matrix blocks as a result of the fracturing process. This solution generalizes previous solutions to model the pressure-transient behavior of partially penetrated wells as proposed in the technical literature for the classical Euclidean formulation, which considers a uniform distribution of fractures that are fully connected. Several synthetic cases obtained with the proposed solution are shown to illustrate the influence of different variables, including fractal parameters.

Keywords: fractal analytical solution; partially penetrated well; single-porosity; naturally fractured reservoir; well test analysis

1. Introduction

In the literature, several analytical solutions for modeling the behavior of pressure-transient tests of partially penetrated wells have been proposed [1–10]. Some of these works have proposed the use of point and line source solutions derived in the Laplace space, considering finite and infinite systems, with homogeneous and naturally fractured reservoirs [2,5,6,8,10]. Other studies considered gas anisotropic reservoirs using a uniform flow solution [9]. All of these works assumed reservoirs with Euclidean geometry, that is, they used traditional mass conservation and flow equations.

Starting from mass conservation and flow equations with fractal characteristics, the authors of [11–14] analyzed the behavior of the pressure-transient tests of single and double porosity reservoirs with fractal geometry. These studies established the existence of a power-law behavior during the transient period instead of the classical semi-logarithmic behavior that exists in reservoirs with Euclidean geometry. It has been demonstrated that the radial flow regime is a special case of more general fractal behavior. All these studies considered vertical fully penetrated wells. Up to date, no study has been presented that considers the pressure-transient behavior of partially penetrated wells produced from anisotropic heterogeneous reservoirs with fractal properties.

In this study, a single-porosity system was considered, which can be represented by a naturally fractured reservoir with a tight matrix, where the porosity and permeability of the system are due to the fracture network. Additionally, it was considered that there was a folding where the density of fractures was greater at the top of the anticline and decreased toward the flanks. Thus, there was a heterogeneous and anisotropic reservoir where the radial and vertical permeabilities were functions of the radial and vertical position, respectively. Due to the complexity of this fracture network, it was convenient to consider fractal geometry, instead of assuming a uniform distribution of fractures, and all fractures as being interconnected, as is considered in the traditional formulation with Euclidean geometry.

The purpose of this work was to obtain an analytical solution that represented the behavior of pressure-transient tests in vertical wells partially penetrating heterogeneous and anisotropic reservoirs with fractal geometry. The heterogeneity and anisotropy were due to a fracture network caused by the thrust of a salt dome.

2. Problem Statement

The solution proposed in this study considered a closed cylindrical reservoir with a single porosity, i.e., a network of fractures may exist, but the matrix is compact and does not contribute to the reservoir response. The well was produced from a restricted interval of the formation. In the reservoir, there were fractal distributions of permeability and porosity in the radial and vertical directions, that is, it was a heterogeneous and anisotropic reservoir. Using the continuity equation in cylindrical coordinates:

$$\frac{1}{r}\frac{\partial}{\partial r}\left(r\rho v_r\right)+\frac{\partial}{\partial z}\left(\rho v_z\right)=-\frac{\partial\left(\rho\phi\right)}{\partial t}, \tag{1}$$

considering a distribution of permeability in the fracture network like that existing in an anticline, where the radial permeability decreases as the radial distance from the center of the anticline increases, and the vertical permeability also decreases with the increment of vertical depth from the top of the anticline. Thus, the fractal distribution of permeability in the radial and vertical directions are given as follows:

$$k_r = k_{rw}\left(\frac{r}{r_w}\right)^{d_{fr}-\theta_r-D_r}, \tag{2}$$

$$k_z = k_{zw}\left(\frac{z}{r_w}\right)^{d_{fz}-\theta_z-D_z}, \tag{3}$$

where k_{rw} and k_{zw} represent the radial permeability at the center and the vertical permeability at the top of the anticline, respectively. $D_r = 2$ and $D_z = 1$ are the Euclidean dimensions in the horizontal and vertical directions, respectively. The fracture density is represented by the fractal dimensions d_{fr} and d_{fz}, in the radial and vertical directions, respectively. θ_r and θ_z represent the connectivity indexes of the fracture network in the radial and vertical directions, respectively. The definition of radial permeability is similar to that used in References [11–14].

The porosity of the fracture network is also a function of the radial distance from the center of the anticline and the vertical position from the top of the anticline. Thus, using the fractal definition of porosity proposed by Cossio et al. [15] in 2D (r and z), the fracture porosity is given by:

$$\phi_f = \frac{\overline{\phi}_0}{2}\left[\left(\frac{r}{r_w}\right)^{d_{fr}-D_r}+\left(\frac{z}{r_w}\right)^{d_{fz}-D_z}\right], \tag{4}$$

where $\overline{\phi}_0$ represents the average porosity in the near wellbore region at the top of the reservoir. In the following, we use $\phi_0 = \overline{\phi}_0/2$.

Assuming Darcy´s Law for the velocities in the radial and vertical directions and considering Equations (2)–(4) into Equation (1), the following equation can be obtained:

$$\frac{1}{r}\frac{\partial}{\partial r}\left(r\rho\frac{k_{rw}(r/r_w)^{d_{fr}-\theta r-Dr}}{\mu}\frac{\partial p}{\partial r}\right)+\frac{\partial}{\partial z}\left(\rho\frac{k_{zw}(z/r_w)^{d_{fz}-\theta_z-D_z}}{\mu}\frac{\partial p}{\partial z}\right)=\frac{\partial}{\partial t}\left(\rho\phi_0\left[\left(\frac{r}{r_w}\right)^{d_{fr}-D_r}+\left(\frac{z}{r_w}\right)^{d_{fz}-D_z}\right]\right). \quad (5)$$

It can be noted that instead of fractal derivatives, fractal definitions of the petrophysical properties are used in the derivation of this equation, following a similar path to that proposed in References [11–17]. Some applications of the use of fractional derivatives on the fluid flow in porous media are presented elsewhere [18–21]. Using the values of the Euclidean dimensions in the horizontal and vertical directions, $D_r = 2$ and $D_z = 1$, we obtained the following equation:

$$\frac{1}{r}\frac{\partial}{\partial r}\left(r\rho\frac{k_{rw}(r/r_w)^{d_{fr}-\theta r-2}}{\mu}\frac{\partial p}{\partial r}\right)+\frac{\partial}{\partial z}\left(\rho\frac{k_{zw}(z/r_w)^{d_{fz}-\theta_z-1}}{\mu}\frac{\partial p}{\partial z}\right)=\frac{\partial}{\partial t}\left(\rho\phi_0\left[\left(\frac{r}{r_w}\right)^{d_{fr}-2}+\left(\frac{z}{r_w}\right)^{d_{fz}-1}\right]\right). \quad (6)$$

Using the following definitions of dimensionless variables:

$$r_D = r/r_w. \quad (7)$$

$$z_D = z/h. \quad (8)$$

$$h_D = h/rw. \quad (9)$$

$$z_{wD} = z_w/h. \quad (10)$$

$$z_{wmD} = (z_w + h_p/2)/h. \quad (11)$$

$$h_{wD} = h_w/h. \quad (12)$$

$$h_{pD} = h_p/h. \quad (13)$$

$$\beta_r = d_{fr} - \theta_r - 1. \quad (14)$$

$$\beta_z = d_{fz} - \theta_z - 1. \quad (15)$$

$$\varepsilon = k_{zw}/k_{rw}. \quad (16)$$

$$t_D = \frac{k_{rw}t}{\phi_0\mu c_t r_w^2}. \quad (17)$$

$$p_D = \frac{2\pi k_{rw}h(p_i - p)}{qB\mu}. \quad (18)$$

Considering a slightly compressible fluid of constant viscosity (μ), and small pressure gradients, we obtained:

$$\frac{1}{r_D}\frac{\partial}{\partial r_D}\left(r_D^{\beta_r}\frac{\partial p_D}{\partial r_D}\right)+\varepsilon h_D^{\beta_z-2}\frac{\partial}{\partial z_D}\left(z_D^{\beta_z}\frac{\partial p_D}{\partial z_D}\right)=\left[r_D^{d_{fr}-2}+(h_D z_D)^{d_{fz}-1}\right]\frac{\partial p_D}{\partial t_D}. \quad (19)$$

In Figure 1, a diagram of the problem to be solved in cylindrical coordinates is shown.

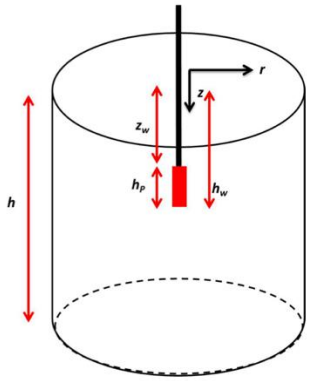

Figure 1. Problem in cylindrical coordinates.

Applying Newman's method according to Razminia et al. [10], "the instantaneous Green function is equal to the product of the instantaneous Green functions in one and/or two directions", in our case:

$$S(r_D, z_D, t_D) = S_r(r_D, t_D) \cdot S_z(z_D, t_D) \quad (20)$$

With the above, Equation (19) will be solved for the two directions independently.

3. Analytical Solution of the Problem

The solution was deduced by applying the methods of the Laplace's transform, separation of variables, and Newman's product using instantaneous source functions. In Appendix A, the procedure for obtaining the solution in the radial direction for total penetration, Equation (A.7), can be found. This solution was used together with the solution in the vertical direction, Equation (B.18), obtained in Appendix B, to acquire the solution for a partially penetrated well through the use of the Newman's product. Thus, Equation (B.26) is written as follows:

$$\bar{p}_{wD}(s) = \frac{2}{h_{pD}^2 \cdot s} \cdot \sum_{n=0}^{\infty} \frac{K_{v_r}[\psi_n]\left\{ z_{wD}^{\frac{d_{fz}}{2}} J_{v_z-1}\left(a_n z_{wD}^{\frac{(2+\theta_z)}{2}} \right) - h_{wD}^{\frac{d_{fz}}{2}} J_{v_z-1}\left(a_n h_{wD}^{\frac{(2+\theta_z)}{2}} \right) \right\}^2}{\left[\sqrt{s+\lambda_n} \left(\frac{1}{2} \right) \left[K_{v_r-1}[\psi_n] + K_{v_r+1}[\psi_n] \right] - \left(\frac{1-\beta_r}{2} \right) K_{v_r}[\psi_n] \right] a_n^2 \left[J_{v_z-1}(a_n) - \frac{v_z}{a_n} J_{v_z}(a_n) \right]^2}, \quad (21)$$

where:

$$\psi_n = \left(\frac{2}{2+\theta_r} \right) \sqrt{s+\lambda_n}. \quad (22)$$

If this expression is evaluated for $h_{pD} = 1, z_{wD} = 0$, and $h_{wD} = 1$, we obtain the fully-penetrated well solution:

$$\begin{aligned} \bar{p}_{wD}(s) = & \frac{K_{v_r}\left[\left(\frac{2}{2+\theta_r} \right) \sqrt{s} \right]}{s \left[\sqrt{s} \left(\frac{1}{2} \right) \left[K_{v_r-1}\left[\left(\frac{2}{2+\theta_r} \right) \sqrt{s} \right] + K_{v_r+1}\left[\left(\frac{2}{2+\theta_r} \right) \sqrt{s} \right] \right] - \left(\frac{1-\beta_r}{2} \right) K_{v_r}\left[\left(\frac{2}{2+\theta_r} \right) \sqrt{s} \right] \right]} \\ & + \frac{2}{h_{pD}^2 \cdot s} \cdot \sum_{n=1}^{\infty} \frac{K_{v_r}[\psi_n]\left\{ z_{wD}^{\frac{d_{fz}}{2}} J_{v_z-1}\left(a_n z_{wD}^{\frac{(2+\theta_z)}{2}} \right) - h_{wD}^{\frac{d_{fz}}{2}} J_{v_z-1}\left(a_n h_{wD}^{\frac{(2+\theta_z)}{2}} \right) \right\}^2}{\left[\sqrt{s+\lambda_n} \left(\frac{1}{2} \right) \left[K_{v_r-1}[\psi_n] + K_{v_r+1}[\psi_n] \right] - \left(\frac{1-\beta_r}{2} \right) K_{v_r}[\psi_n] \right] a_n^2 \left[J_{v_z-1}(a_n) - \frac{v_z}{a_n} J_{v_z}(a_n) \right]^2}. \end{aligned} \quad (23)$$

where λ_n are the characteristic values given by the roots of Equation (B.10), and:

$$a_n = \frac{2}{2+\theta_z}\sqrt{\frac{\lambda_n h_D^{2+\theta_z}}{\varepsilon}}\,. \tag{24}$$

The second term of Equation (23) represents the pseudo-skin due to partial penetration considering fractal behavior in both radial and vertical directions.

To include wellbore storage and mechanical skin effects, the following expression, given by Van Everdingen and Hurst [22], is applied:

$$\bar{p}_{wD}(s) = \frac{s\bar{p}_D(s)+S}{s+C_D s^2\left[s\bar{p}_D(s)+S\right]}. \tag{25}$$

where $\bar{p}_D(s)$ is given by Equation (23).

4. Results

In this section, some results are presented with the proposed analytical solution given by Equations (23) and (25) in the case of wellbore storage and skin effects using Stehfest's algorithm [23].

Figures 2–5 show the solution for a Euclidean isotropic case (d_{fr} = 2.0, θ_r = 0, d_{fz} = 1.0, θ_z = 0), where the upper part of the formation is open to production. Figure 2 shows results without mechanical skin damage, S = 0, where only the thickness of the formation varies. The dashed lines in Figures 2–5 correspond to the pressure and pressure derivative given by Razminia et al. [10] for some Euclidian cases. In all cases, the agreement is excellent, so the proposed solution, Equation (23), is able to reproduce the Euclidian results as particular cases.

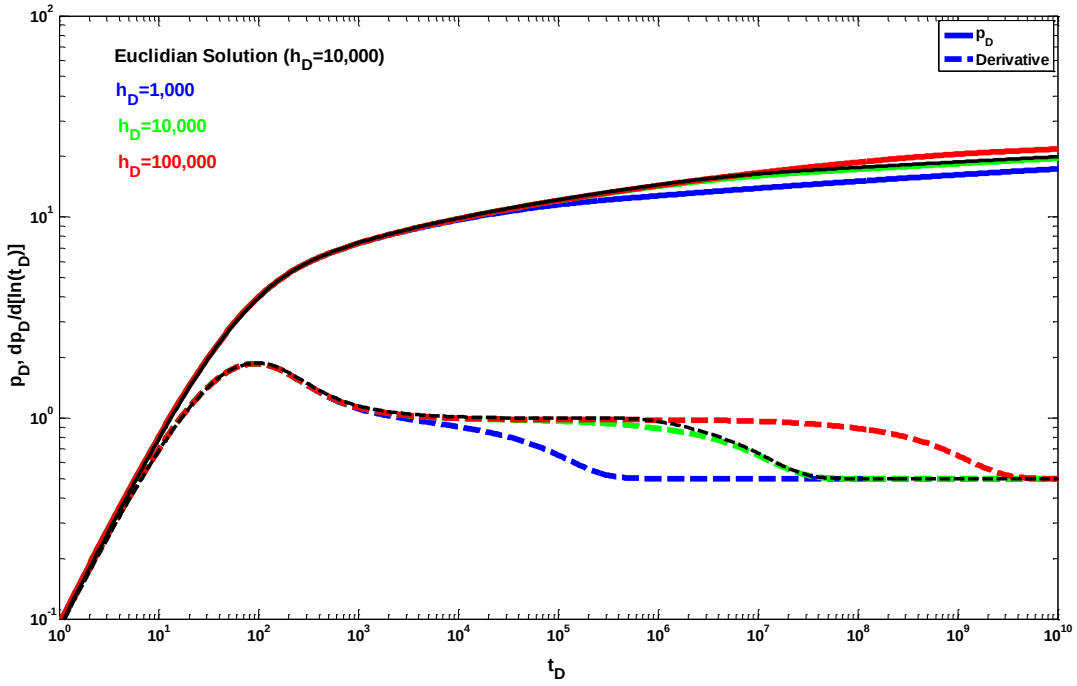

Figure 2. Euclidean case: $z_{wD} = 0$, $h_{pD} = 0.5$, $S = 0$, $C_D = 10$, $\varepsilon = 1, d_{fr} = 2$, $\theta_r = 0$, $d_{fz} = 1$, $\theta_z = 0$.

In Figure 3, the magnitude of the open interval varies, including the case of the fully penetrated well, keeping the thickness of the formation constant. In Figures 4 and 5, the mechanical skin damage and wellbore storage vary, respectively, keeping the thickness of the formation and the open interval constant. All these cases are Euclidean and serve to evaluate the accuracy of the fractal analytic solution proposed for these cases.

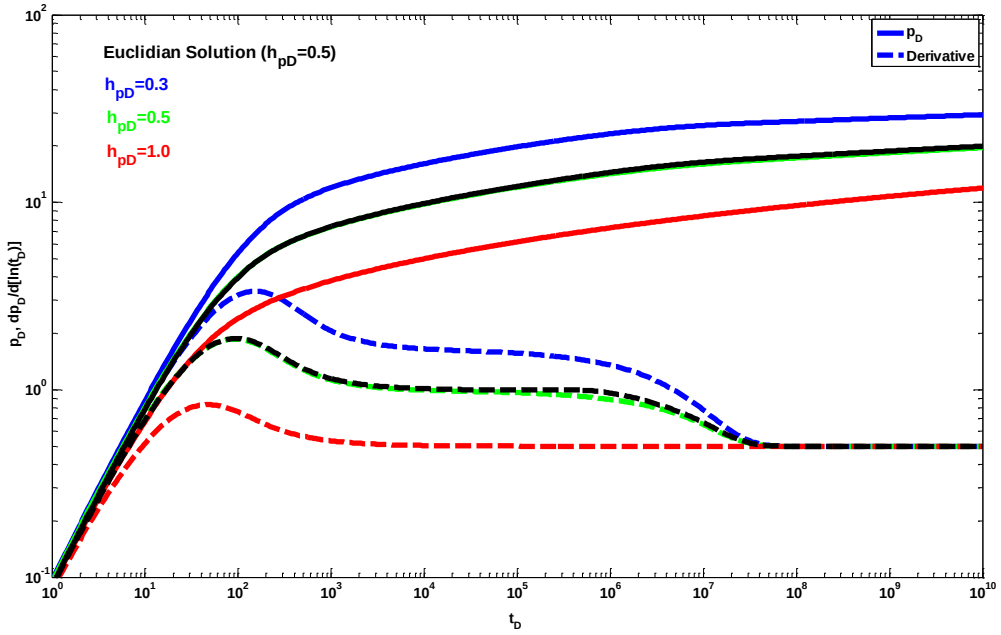

Figure 3. Euclidean case: $z_{wD} = 0,\ h_D = 10{,}000,\ S = 0,\ C_D = 10,\ \varepsilon = 1, d_{fr} = 2,\ \theta_r = 0,\ d_{fz} = 1,\ \theta_z = 0.$

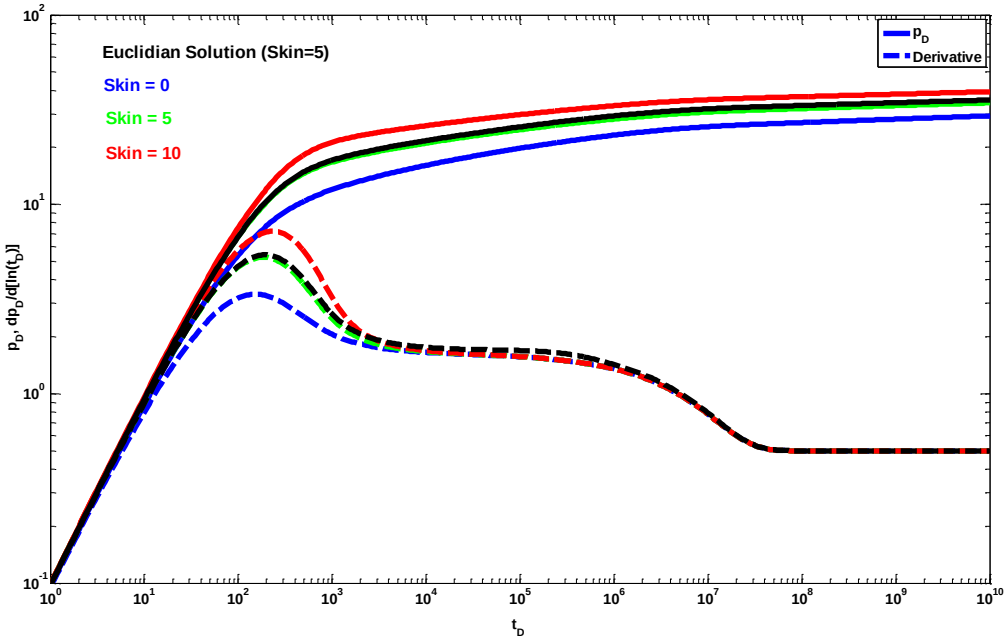

Figure 4. Euclidean case: $z_{wD} = 0,\ h_D = 10{,}000,\ h_{pD} = 0.3,\ C_D = 10,\ \varepsilon = 1, d_{fr} = 2,\ \theta_r = 0,\ d_{fz} = 1,\ \theta_z = 0.$

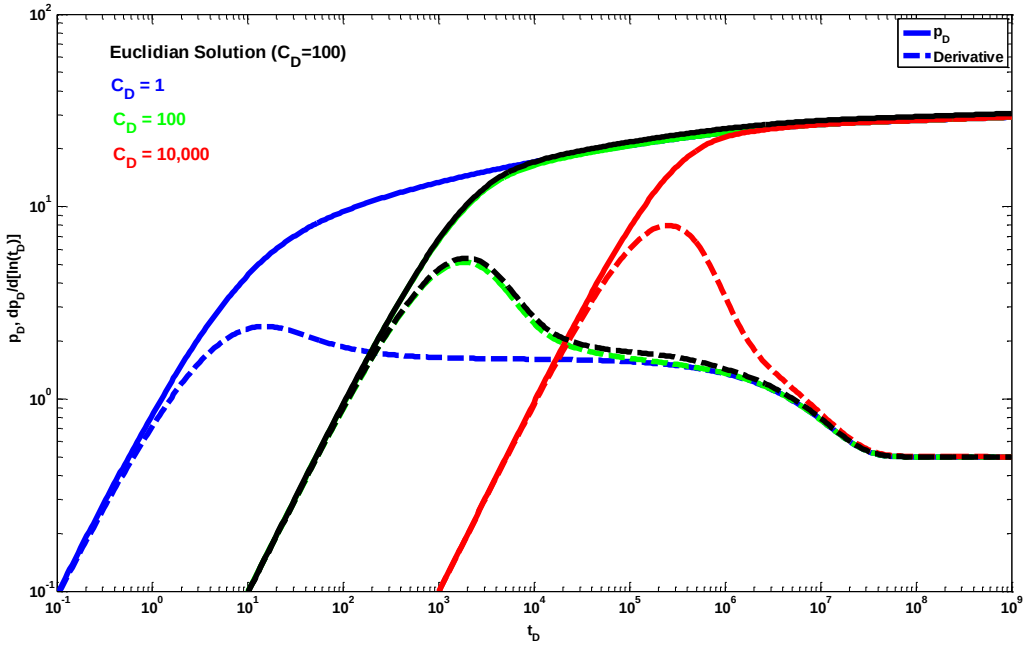

Figure 5. Euclidean case: $z_{wD} = 0,\ h_D = 10{,}000,\ h_{pD} = 0.3,\ S = 1,\ \varepsilon = 1, d_{fr} = 2,\ \theta_r = 0,\ d_{fz} = 1,$ $\theta_z = 0.$

The cases with fractal geometry are shown below. Figure 6 shows a case where the fractal dimension in the radial direction is varying, $d_{fr} \leq 2$, where the value of 2 represents the Euclidean case ($\theta_r = 0$). Thus, the traditional Euclidean case is a special case of the fractal case. In the Euclidean case, the classical spherical flow with a slope of −0.5, before the radial period, is present. It can be observed that this period of flow is not present for the fractal cases, where instead of the semi-logarithmic period, a power-law behavior can be observed in both the pressure drop and its derivative at late times during the transient period.

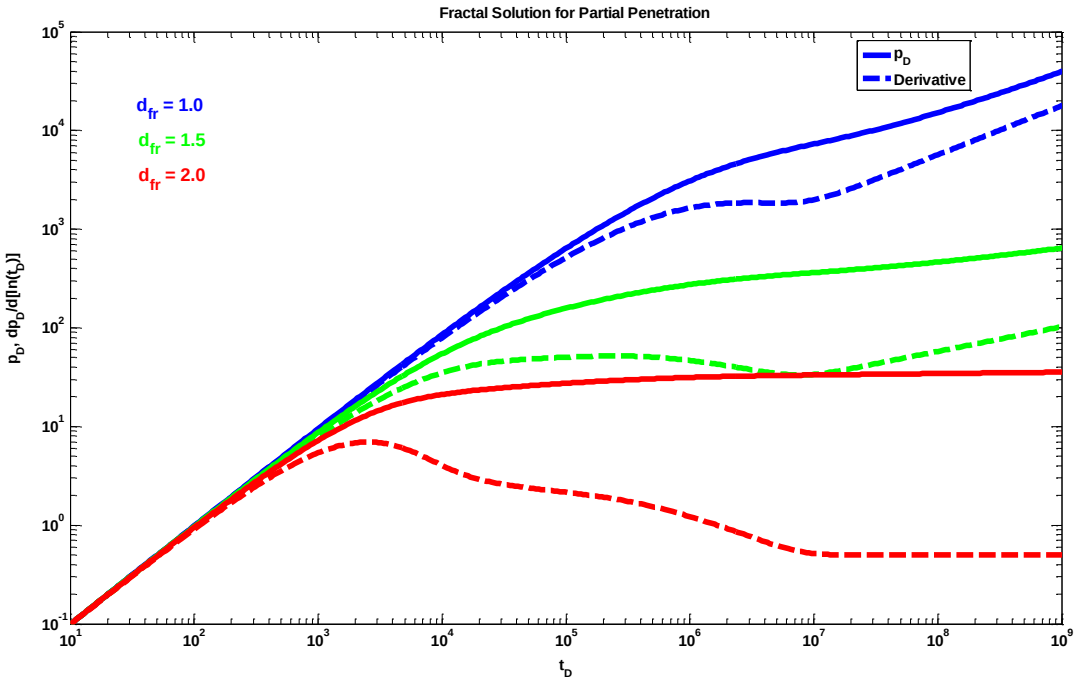

Figure 6. Fractal case: $z_{wD} = 0.4,\ h_D = 10000,\ h_{pD} = 0.2\ S = 0,\ C_D = 100,\ \varepsilon = 1,\ \theta_r = 0,\ d_{fz} = 1,$ $\theta_z = 0.$

Figure 7 shows fractal cases where the connectivity index in the radial direction (θ_r) varies, and now all other parameters are kept constant, including the fractal dimension d_{fr} = 2. Again, the Euclidean case occurs when θ_r = 0, i.e., radial flow exists at late times during the transient period, and when $\theta_r > 0$, the power-law response is present at these times.

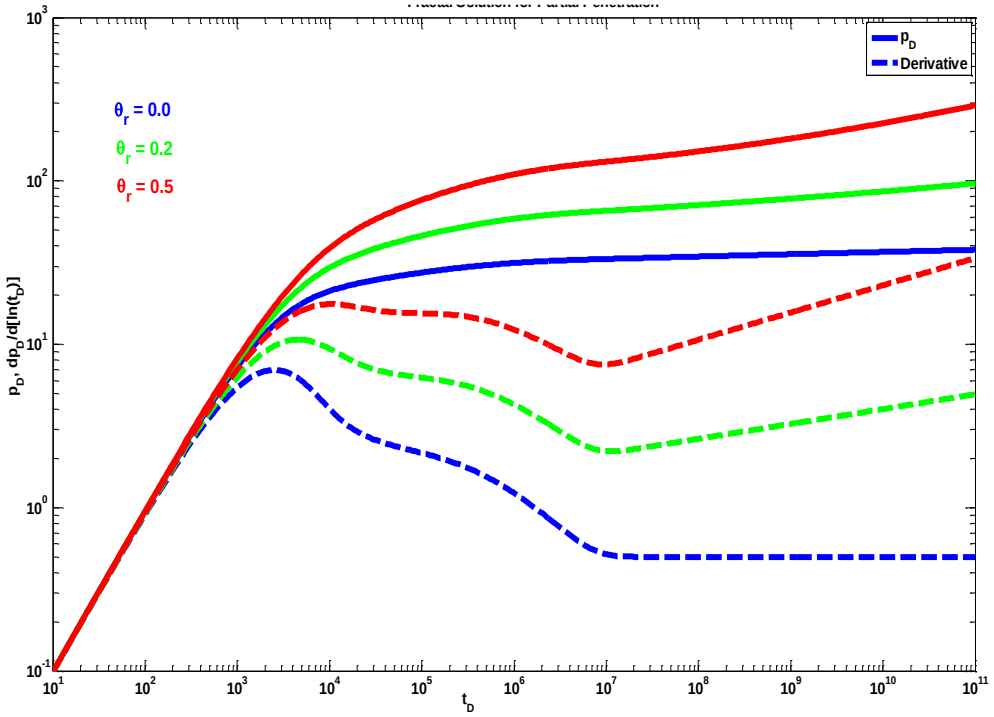

Figure 7. Fractal case: $z_{wD} = 0.4$, $h_D = 10000$, $h_{pD} = 0.2$ S = 0, $C_D = 100$, $\varepsilon = 1$, $d_{fr} = 2$, $d_{fz} = 1$, $\theta_z = 0$.

In Figures 8 and 9 the fractal dimension, d_{fz}, and the connectivity index, θ_z, are varied in the vertical direction, respectively, keeping the other parameters constant, including d_{fr} = 2, and θ_r = 0. The influence of d_{fz} and θ_z is observed only in the period before the radial flow. In these cases, when d_{fz} = 1.0 and θ_z = 0, the traditional Euclidean case is obtained again, with the presence of spherical flow before the radial period.

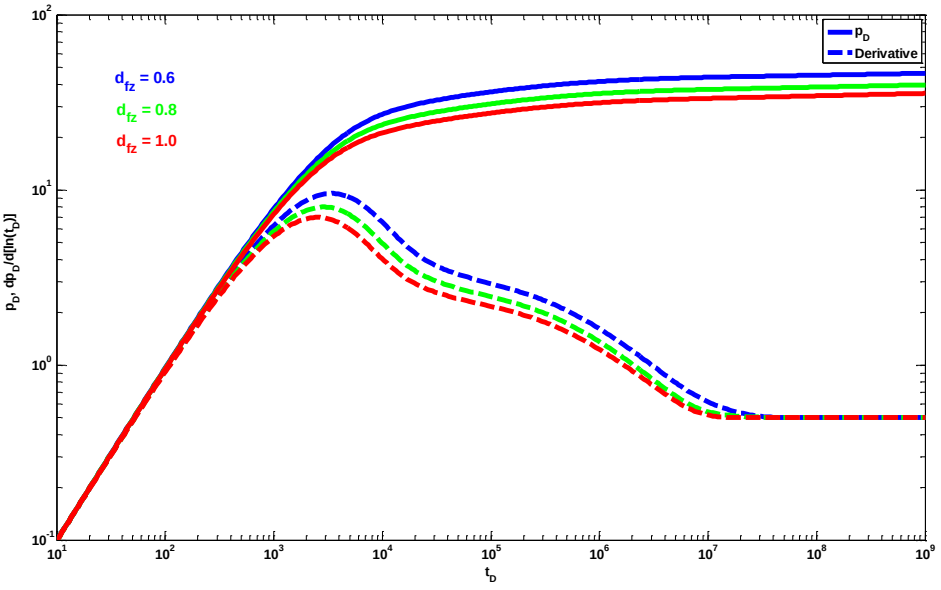

Figure 8. Fractal case: $z_{wD} = 0.4,\ h_D = 10{,}000,\ h_{pD} = 0.2,\ S = 0,\ C_D = 100,\ \varepsilon = 1,\ d_{fr} = 2.0,$ $\theta_r = 0,\ \theta_z = 0.$

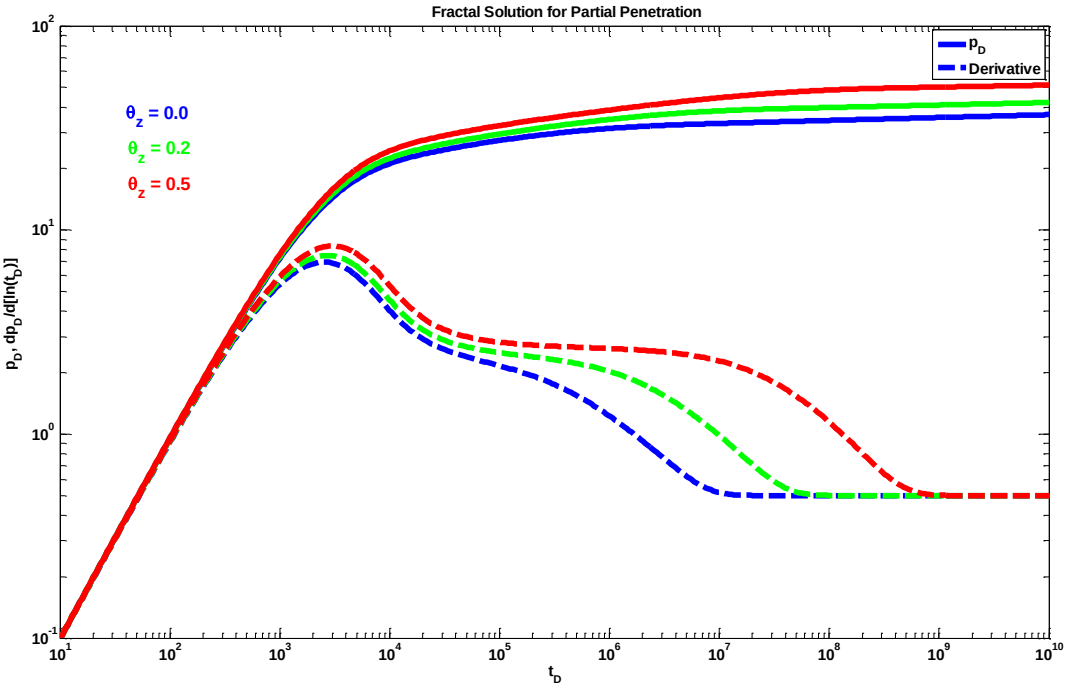

Figure 9. Fractal case: $z_{wD} = 0.4,\ h_D = 10{,}000,\ h_{pD} = 0.2,\ S = 0,\ C_D = 100,\ \varepsilon = 1,\ d_{fr} = 2.0,$ $\theta_r = 0,\ d_{fz} = 1.0.$

In Figures 10 and 11, the influence of h_{pD} and the mechanical skin is shown, respectively, keeping the other parameters constant, including the fractal parameters. At large times within the transient period, the power-law behavior can be detected. In fact, in Figure 11, the presence of two power-law periods is observed.

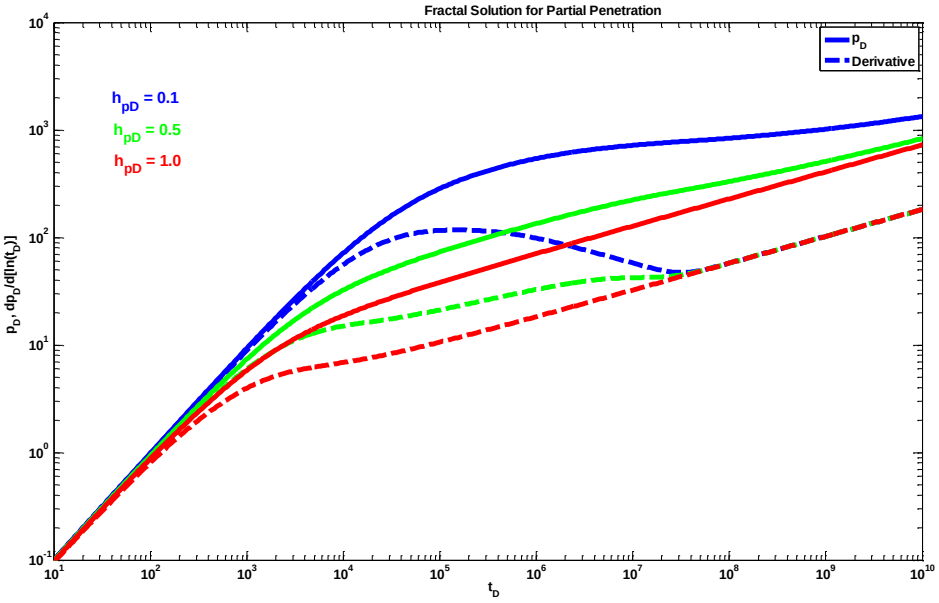

Figure 10. Fractal case: $z_{wD} = 0,\ h_D = 10{,}000,\ S = 0,\ C_D = 100,\ \varepsilon = 1, d_{fr} = 1.5,\ \theta_r = 0,\ d_{fz} = 1.0,$ $\theta_z = 0.$

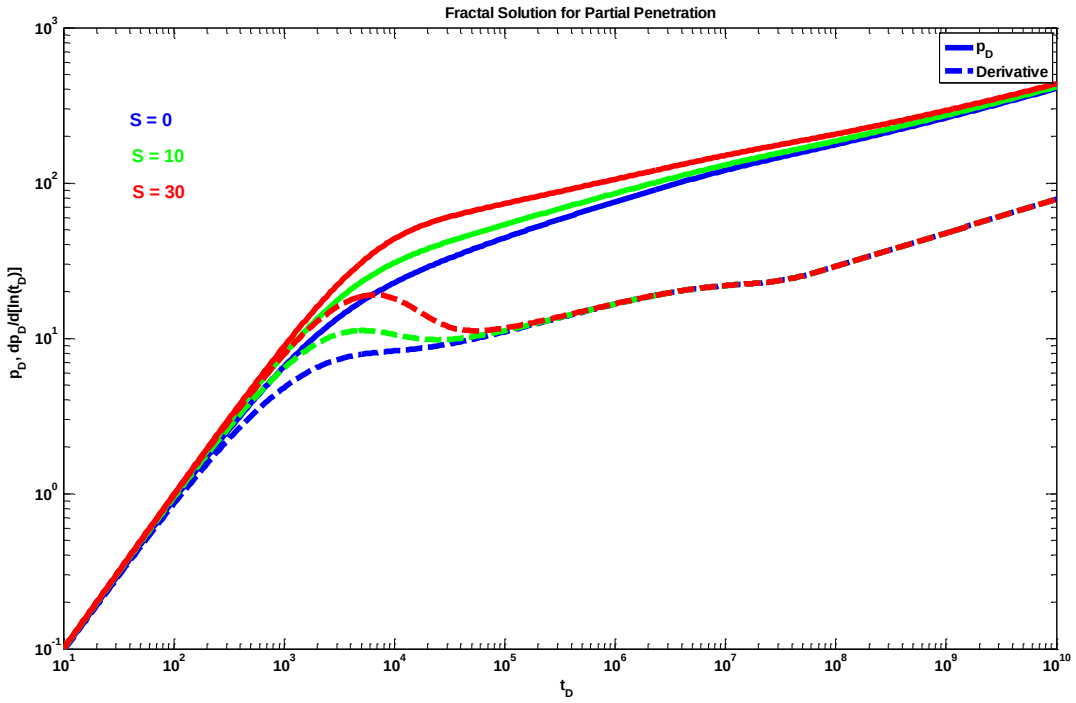

Figure 11. Fractal case: $z_{wD} = 0.2$, $h_{pD} = 0.6$, $h_D = 10{,}000$, $C_D = 100, \varepsilon = 1$, $d_{fr} = 1.8$, $\theta_r = 0.3$, $d_{fz} = 1.0$, $\theta_z = 0.2$.

Figures 12 and 13 show the influence of the fractal parameters in the vertical direction, considering a fractal condition in the radial direction. In Figure 12, it is observed that the effect of the fractal dimension, d_{fz}, is not very strong; however, it can be expected that with the arrival of undesirable fluids to the producing well, this parameter could play an important role. In both figures, the presence of two power-law periods is observed. Figure 13 shows that when the connectivity of fractures or pores in the vertical direction decreases, or even becomes null (i.e., θ_z = 1), the late power-law period is delayed, which is an expected behavior.

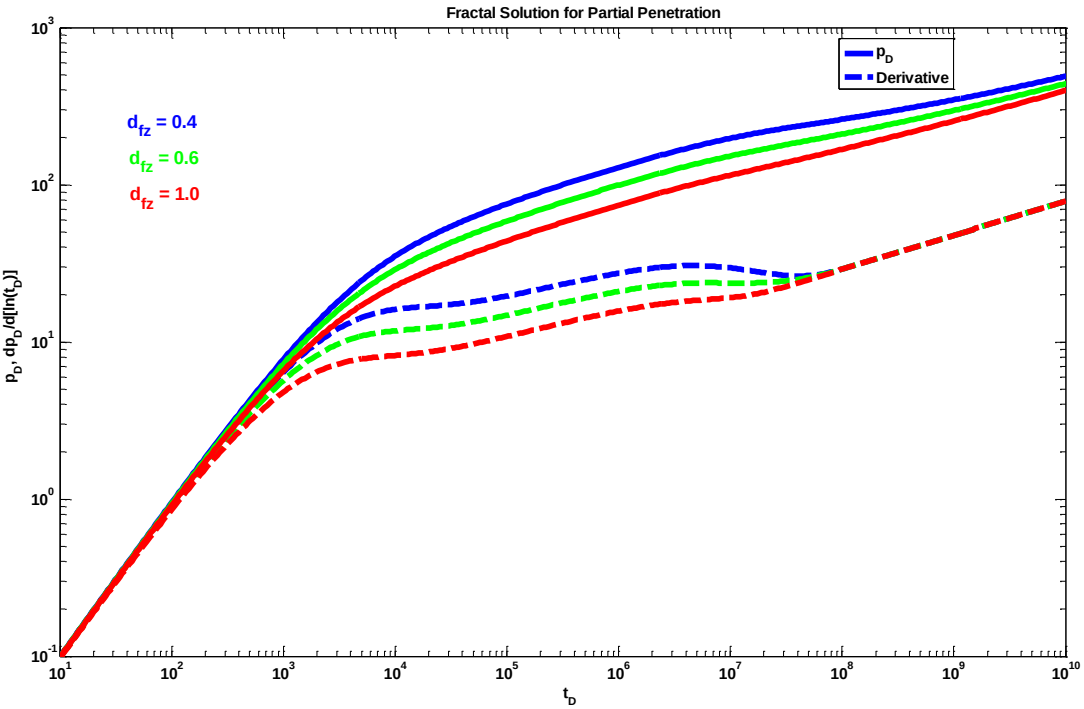

Figure 12. Fractal case: $z_{wD} = 0.2,\ h_{pD} = 0.6,\ h_D = 10{,}000,\ S = 0,\ C_D = 100,\ \varepsilon = 1, d_{fr} = 1.8,$ $\theta_r = 0.3,\ \theta_z = 0.1.$

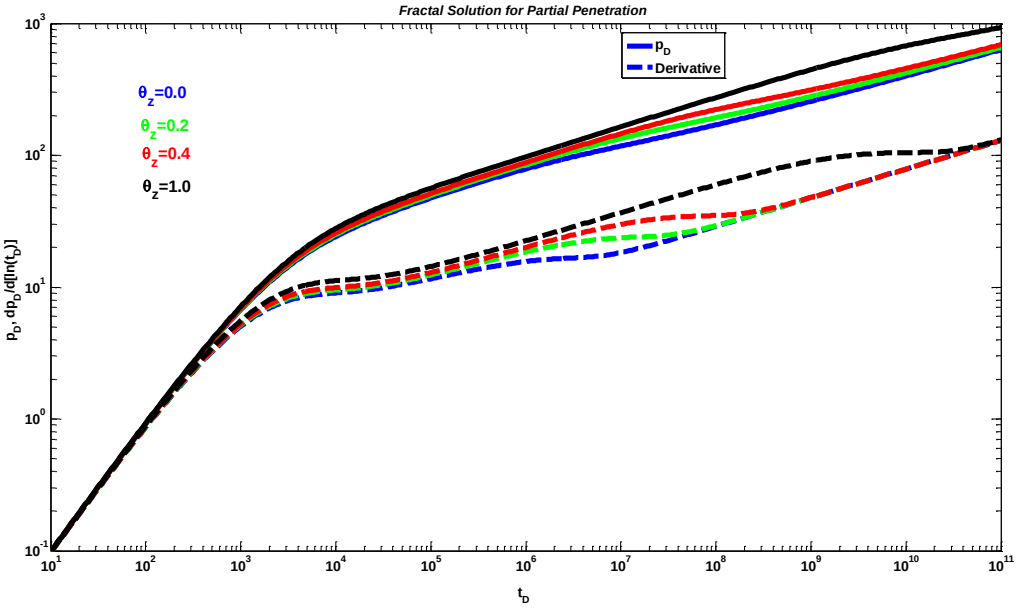

Figure 13. Fractal case: $z_{wD} = 0.2,\ h_{pD} = 0.6,\ h_D = 10{,}000,\ S = 0,\ C_D = 100,\ \varepsilon = 1, d_{fr} = 1.8,$ $\theta_r = 0.3,\ d_{fz} = 0.8.$

Considering the above results, it can be deduced that the new proposed analytical solution may provide useful information for the proper development of a reservoir. However, it can be intuited that to determine all the parameters involved in the proposed analytical solution, it is necessary to use a robust optimizer, since a visual adjustment is expected to be very difficult to apply for a complex model such as the one proposed in this work.

5. Discussion

Taking into account the above results, and those presented by Posadas and Camacho [14], and the fact that there are many unknown parameters (S, C_D, ε, d_{fr}, θ_r, d_{fz}, θ_z, k_r) to fully characterize this system, it is necessary to use robust optimization software in the type–curve matching process of both the pressure and its semi-logarithmic pressure derivative in order to obtain all of these parameters from well test data.

6. Conclusions

The novel analytical solution presented in this paper considers for the first time the application of fractal geometry to the problem of partial penetration. This is relevant because it allows the consideration of the variation of petrophysical properties with the scale or it takes into account the tortuosity of the flow lines in a cylindrical system. The solution was deduced by applying the methods of the Laplace's transform, separation of variables, and Newman's product using instantaneous source functions. Considering the results presented in this article, we can conclude the following:

1. The new fractal analytical solution for a constant rate describes the pressure-transient behavior for partially penetrating wells in a single-porosity naturally fractured reservoir and includes the traditional Euclidean solution as a special case.
2. The proposed fractal solution generates a power-law response at late times during the transient period after the wellbore storage, mechanical skin, and partial penetration effects have ended. This behavior occurs when the radial fractal parameters are different from the Euclidean values, i.e., $d_{fr} < 2$ and $\theta_r > 0$.

3. A different behavior to the power-law response occurs when $d_{fz} < 1$ and $\theta_z > 0$. The effect of these parameters is shown only during the partial penetration period, and after this period, the traditional radial behavior (if $d_{fr} = 2$ and $\theta_r = 0$) or a power-law behavior (when $d_{fr} < 2$ and/or $\theta_r > 0$) can be present.
4. The typical spherical flow regime due to partial penetration is only present when the fractal parameters in the radial direction have the Euclidean values, i.e., $d_{fr} = 2$ and $\theta_r = 0$.
5. An expression is provided to evaluate the pseudo-skin due to the partial penetration effects that consider fractal behavior in both the radial and vertical directions.
6. To determine the pseudo-damage due to restricted penetration, horizontal permeability, vertical to horizontal permeability ratio, mechanical skin, and the four fractal parameters, it is necessary to resort to a type–curve matching process of the pressure data and its semi-logarithmic derivative using a robust optimizer that minimizes the difference between the real data and the analytical solution.

Nomenclature

c_t Compressibility [psi^{-1}]
C Wellbore storage constant [bbl/psi]
C_D Dimensionless wellbore storage constant
d_{fr} Fractal dimension in the radial direction ($1 \le d_{fr} \le 2$)
d_{fz} Fractal dimension in the vertical direction ($0 \le d_{fz} \le 1$)
h Formation thickness [ft]
h_p Producing interval [ft]
h_{pD} Dimensionless producing interval
h_{wD} Dimensionless depth at bottom of producing interval
k_r Permeability in the radial direction, [mD]
k_z Permeability in the vertical direction, [mD]
k_{rw} Reference radial permeability at the wellbore, [mD]
k_{zw} Reference vertical permeability at the top of the anticline, [mD]
K_ν Modified Bessel function of order ν
J_ν Bessel function of order ν
p Pressure, [psi]
p_i Initial pressure, [psi]
p_{wD} Dimensionless wellbore pressure
q Production rate, [bpd]
r_w Wellbore radius, [ft]
r_D Dimensionless radius
s Laplace domain parameter
S Mechanical skin factor
t Time, [hours]
t_D Dimensionless time
z Vertical depth from the top of the dome, [ft]
z_D Dimensionless vertical depth
z_w Top position of open interval, [ft]
z_{wD} Dimensionless depth at top of open interval
z_{wmD} Dimensionless depth at medium of open interval
μ Fluid viscosity, [cp]
ϕ Porosity
θ_r Connectivity index in the radial direction ($0 \le \theta_r \le 1$)
θ_z Connectivity index in the vertical direction ($0 \le \theta_z \le 1$)
$\xi(s)$ Pseudo-skin due to partial penetration considering fractal behavior

Acknowledgments: The authors appreciate the support of Pemex E&P and the National University of Mexico, UNAM, during the development of this work.

Author Contributions: Ricardo Posadas and Rodolfo Camacho conceived and derived the analytical solutions; Ricardo Posadas performed the numerical experiments; Ricardo Posadas and Rodolfo Camacho analyzed the results; Rodolfo Camacho and Ricardo Posadas wrote the paper.

Conflicts of Interest: The authors declare no conflict of interest.

Appendix A. Solution in the Radial Direction

The flow in the radial direction is obtained from Equation (19) as follows:

$$\frac{1}{r_D}\frac{\partial}{\partial r_D}\left(r_D^{\beta_r}\frac{\partial S_r}{\partial r_D}\right)=r_D{}^{d_{fr}-2}\frac{\partial S_r}{\partial t_D}. \tag{A.1}$$

where $\beta_r = d_{fr} - \theta_r - 1$.

Using the Laplace transform:

$$\frac{\partial^2 \overline{S}_r}{\partial r_D^2}+\frac{\beta_r}{r_D}\frac{\partial \overline{S}_r}{\partial r_D}-sr_D{}^{\theta_r}\overline{S}_r=0. \tag{A.2}$$

Applying the Levedev [24] technique, we are able to obtain the solution in terms of the modified Bessel functions:

$$\overline{S}_r(r_D)=r_D^{\frac{1-\beta_r}{2}}\left\{AI_{v_r}\left[\left(\frac{2}{2+\theta_r}\right)\sqrt{s}\,r_D^{\frac{2+\theta_r}{2}}\right]+BK_{v_r}\left[\left(\frac{2}{2+\theta_r}\right)\sqrt{s}\,r_D^{\frac{2+\theta_r}{2}}\right]\right\}, \tag{A.3}$$

where:

$$v_r=\left(\frac{1-\beta_r}{2+\theta_r}\right). \tag{A.4}$$

Using the following boundary conditions in the radial direction:

$$\lim_{r_D\to\infty}\overline{S}_r(r_D,s)=0, \tag{A.5}$$

$$\left(r_D\frac{\partial \overline{S}_r}{\partial r_D}\right)_{r_D=1}=-\frac{1}{s}. \tag{A.6}$$

It is found that the solution in the radial direction for total penetration in the Laplace space is given by:

$$\overline{S}_r(r_D,s)=\frac{r_D^{\frac{1-\beta_r}{2}}K_{v_r}\left[\left(\frac{2}{2+\theta_r}\right)\sqrt{s}\,r_D^{\frac{2+\theta_r}{2}}\right]}{s\cdot\left[\sqrt{s}\left(\frac{1}{2}\right)\left[K_{v_r-1}\left[\left(\frac{2}{2+\theta_r}\right)\sqrt{s}\right]+K_{v_r+1}\left[\left(\frac{2}{2+\theta_r}\right)\sqrt{s}\right]\right]-\left(\frac{1-\beta_r}{2}\right)K_{v_r}\left[\left(\frac{2}{2+\theta_r}\right)\sqrt{s}\right]\right]}. \tag{A.7}$$

Appendix B. Solution in the Vertical Direction

From Equation (19), the continuity equation in the vertical direction is given by:

$$z_D^{\beta_z}\frac{d^2S_z}{dz_D^2}+\beta_z z_D^{\beta_z-1}\frac{dS_z}{dz_D}-\left(\frac{h_D^{2+\theta_z}z_D{}^{d_{fz}-1}}{\varepsilon}\right)\frac{\partial S_z}{\partial t_D}=0, \tag{B.1}$$

where $\beta_z = d_{fz} - \theta_z - 1$. Applying separation of variables in Equation (B.1):

$$S_z(z_D,t_D)=w(z_D)u(t_D). \tag{B.2}$$

Thus, the solution for $u(t_D)$ is given by:

$$u(t_D) = Ee^{-\lambda t_D}, \tag{B.3}$$

and the solution for $w(z_D)$ is obtained from:

$$z_D^2 \frac{d^2w}{dz_D^2} + \beta_z z_D \frac{dw}{dz_D} + \frac{\lambda h_D^{2+\theta_z} z_D^{2+\theta_z}}{\varepsilon} w = 0. \tag{B.4}$$

Applying the Levedev [24] technique, we are able to obtain the solution for *w* (z_D), in terms of the Bessel functions:

$$w(z_D) = z_D^{\frac{1-\beta_z}{2}} \left\{ C \cdot J_{v_z}\left[\frac{2}{2+\theta_z} \sqrt{\frac{\lambda h_D^{2+\theta_z}}{\varepsilon}} z_D^{\frac{2+\theta_Z}{2}} \right] + D \cdot Y_{v_z}\left[\frac{2}{2+\theta_z} \sqrt{\frac{\lambda h_D^{2+\theta_z}}{\varepsilon}} z_D^{\frac{2+\theta_Z}{2}} \right] \right\}, \tag{B.5}$$

where:

$$v_z = \frac{1-\beta_z}{2+\theta_Z}. \tag{B.6}$$

Substituting Equations (B.3) and (B.5) into Equation (B.2), the general solution for the problem in the vertical direction is given by:

$$S_z(z_D, t_D) = Ee^{-\lambda t_D} z_D^{\frac{1-\beta_z}{2}} \left\{ C \cdot J_{v_z}\left[\frac{2}{2+\theta_z} \sqrt{\frac{\lambda h_D^{2+\theta_z}}{\varepsilon}} z_D^{\frac{2+\theta_Z}{2}} \right] + D \cdot Y_{v_z}\left[\frac{2}{2+\theta_z} \sqrt{\frac{\lambda h_D^{2+\theta_z}}{\varepsilon}} z_D^{\frac{2+\theta_Z}{2}} \right] \right\}. \tag{B.7}$$

Considering the following boundary conditions in the vertical direction:

$$\frac{\partial S_z(z_D = 0, t_D)}{\partial z_D} = 0, \tag{B.8}$$

$$\frac{\partial S_z(z_D = 1, t_D)}{\partial z_D} = 0. \tag{B.9}$$

We obtain from Equation (B.8), D = 0. From Equation (B.9) we obtain:

$$0 = \sqrt{\frac{\lambda h_D^{2+\theta_z}}{\varepsilon}} \left(\frac{1}{2}\right) \left(J_{v_z - 1}\left[\frac{2}{2+\theta_z} \sqrt{\frac{\lambda h_D^{2+\theta_z}}{\varepsilon}} \right] - J_{v_z + 1}\left[\frac{2}{2+\theta_z} \sqrt{\frac{\lambda h_D^{2+\theta_z}}{\varepsilon}} \right] \right) + \left(\frac{1-\beta_z}{2} \right) J_{v_z}\left[\frac{2}{2+\theta_z} \sqrt{\frac{\lambda h_D^{2+\theta_z}}{\varepsilon}} \right]. \tag{B.10}$$

From the roots of Equation (B.10) the characteristic values λ are obtained.

Applying the superposition principle with Equation (B.7) we obtain the following expression:

$$S_z(z_D, t_D) = \sum_{n=0}^{\infty} C_n \cdot e^{-\lambda_n t_D} z_D^{\frac{1-\beta_z}{2}} \cdot J_{v_z}\left[\frac{2}{2+\theta_z} \sqrt{\frac{\lambda_n h_D^{2+\theta_z}}{\varepsilon}} z_D^{\frac{2+\theta_Z}{2}} \right]. \tag{B.11}$$

Considering an instantaneous source plate with its center in z_{wmD}, which agrees with the midpoint of the producing interval, the following expression is obtained:

$$H\left[z_D - \left(z_{wmD} - h_{pD}/2\right)\right] - H\left[z_D - \left(z_{wmD} + h_{pD}/2\right)\right] = H\left[z_D - z_{wD}\right] - H\left[z_D - h_{wD}\right] = C_n \sum_{n=0}^{\infty} \cdot z_D^{\frac{1-\beta_z}{2}} \cdot J_{v_z}\left[\frac{2}{2+\theta_z} \sqrt{\frac{\lambda_n h_D^{2+\theta_z}}{\varepsilon}} z_D^{\frac{2+\theta_z}{2}} \right] \cdot \tag{B.12}$$

Multiplying Equation (B.12) by $x = z_D^{\frac{2+\theta_z}{2}}$ and then applying the orthogonality property, we obtain:

$$\int_{z_{wmD}-\frac{h_{pD}}{2}}^{z_{wmD}+\frac{h_{pD}}{2}} z_D^{\frac{d_{fz}+\theta_z}{2}} J_{v_z}\left[\frac{2}{2+\theta_z}\sqrt{\frac{\lambda_n h_D^{2+\theta_z}}{\varepsilon}} z_D^{\frac{2+\theta_z}{2}}\right] dz_D = C_n \cdot \int_0^1 \frac{x}{\left(\frac{2+\theta_z}{2}\right)}\left[J_{v_z}\left(\frac{2}{2+\theta_z}\sqrt{\frac{\lambda_n h_D^{2+\theta_z}}{\varepsilon}} x\right)\right]^2 dx \cdot \tag{B.13}$$

To evaluate the term of the integral on the right-hand side of Equation (B.13), Abramowitz and Stegun [25] is used, obtaining the following expression:

$$\int_0^1 \frac{2x}{(2+\theta_z)}\left[J_{v_z}\left(\frac{2}{2+\theta_z}\sqrt{\frac{\lambda_n h_D^{2+\theta_z}}{\varepsilon}} x\right)\right]^2 dx = \frac{1}{(2+\theta_z)}\left[J_{v_z-1}(a_n) - \frac{v_z}{a_n} J_{v_z}(a_n)\right]^2, \tag{B.14}$$

where $a_n = \frac{2}{2+\theta_z}\sqrt{\frac{\lambda_n h_D^{2+\theta_z}}{\varepsilon}}$. To evaluate the term of the integral on the left-hand side of Equation (B.13), we use Gradshteyn and Ryzhik [26], which is expressed as:

$$\int x^{1-v_z} \cdot J_{v_z}[a_n \cdot x] dx = -\frac{x^{1-v_z} J_{v_z-1}(a_n x)}{a_n}. \tag{B.15}$$

Obtaining the following:

$$\left(\frac{2}{2+\theta_z}\right)\int_{\left(z_{wmD}-\frac{h_{pD}}{2}\right)^{(2+\theta_z)/2}}^{\left(z_{wmD}+\frac{h_{pD}}{2}\right)^{(2+\theta_z)/2}} x^{1-v_z} \cdot J_{v_z}[a_n \cdot x] dx = \left(\frac{2}{2+\theta_z}\right)\frac{1}{a_n}\left(\left(z_{wmD}-\frac{h_{pD}}{2}\right)^{\frac{d_{fz}}{2}} J_{v_z-1}\left(a_n\left(z_{wmD}-\frac{h_{pD}}{2}\right)^{(2+\theta_z)/2}\right) - \left(z_{wmD}+\frac{h_{pD}}{2}\right)^{\frac{d_{fz}}{2}} J_{v_z-1}\left(a_n\left(z_{wmD}+\frac{h_{pD}}{2}\right)^{(2+\theta_z)/2}\right)\right). \tag{B.16}$$

Substituting Equations (B.14) and (B.16) into Equation (B.13), we obtain:

$$C_n = \frac{2\left\{z_{wD}^{\frac{d_{fz}}{2}} J_{v_z-1}\left(a_n z_{wD}^{\frac{(2+\theta_z)}{2}}\right) - h_{wD}^{\frac{d_{fz}}{2}} J_{v_z-1}\left(a_n h_{wD}^{\frac{(2+\theta_z)}{2}}\right)\right\}}{a_n\left[J_{v_z-1}(a_n) - \frac{v_z}{a_n} J_{v_z}(a_n)\right]^2}. \tag{B.17}$$

Substituting Equation (B.17) into Equation (B.11), the following solution is obtained:

$$S_z(z_D, t_D) = 2 \cdot \sum_{n=0}^{\infty} \frac{e^{-\lambda_n t_D} z_D^{\frac{1-\beta_z}{2}} \cdot J_{v_z}\left[a_n z_D^{\frac{2+\theta_z}{2}}\right]\left\{z_{wD}^{\frac{d_{fz}}{2}} J_{v_z-1}\left(a_n z_{wD}^{\frac{(2+\theta_z)}{2}}\right) - h_{wD}^{\frac{d_{fz}}{2}} J_{v_z-1}\left(a_n h_{wD}^{\frac{(2+\theta_z)}{2}}\right)\right\}}{a_n\left[J_{v_z-1}(a_n) - \frac{v_z}{a_n} J_{v_z}(a_n)\right]^2}. \tag{B.18}$$

According to Razminia et al. [10] the instantaneous source function for a partial penetration is defined as a function of the instantaneous source function for total penetration, such as:

$$S(r_D, t_D) = \frac{1}{h_{pD}} S(r_D, t_D)_f = \frac{1}{h_{pD}} \frac{\partial p_{Df}(r_D, t_D)}{\partial t_D}. \tag{B.19}$$

Using the method of Newman's product, the instantaneous source function for partial penetration can be obtained as follows:

$$S(r_D, z_D, t_D) = S_r(r_D, t_D) \cdot S_z(z_D, t_D). \tag{B.20}$$

Thus, using Equations (B.18) and (B.19) into Equation (B.20):

$$S(r_D, z_D, t_D) = \frac{2}{h_{pD}} \frac{\partial p_{Df}(r_D, t_D)}{\partial t_D} \cdot \sum_{n=0}^{\infty} \frac{e^{-\lambda_n t_D} z_D^{\frac{1-\beta_z}{2}} J_{v_z}\left[a_n z_D^{\frac{2+\theta_z}{2}}\right]\left\{z_{wD}^{\frac{d_{fz}}{2}} J_{v_z-1}\left(a_n z_{wD}^{\frac{(2+\theta_z)}{2}}\right) - h_{wD}^{\frac{d_{fz}}{2}} J_{v_z-1}\left(a_n h_{wD}^{\frac{(2+\theta_z)}{2}}\right)\right\}}{a_n\left[J_{v_z-1}(a_n) - \frac{v_z}{a_n} J_{v_z}(a_n)\right]^2}. \tag{B.21}$$

Considering that:

$$p_{Df}(r_D, z_D, t_D) = \int_0^{t_D} S(r_D, z_D, \tau) d\tau \,, \tag{B.22}$$

the solution in the Laplace space is given by:

$$\bar{p}_D(r_D, z_D, s) = \frac{2}{h_{pD} \cdot s} \cdot \sum_{n=0}^{\infty} \frac{(s+\lambda_n)\bar{p}_{Df}(r_D, s+\lambda_n) z_D^{\frac{1-\beta_z}{2}} J_{v_z}\left[a_n z_D^{\frac{2+\theta_z}{2}}\right]\left\{z_{wD}^{\frac{d_{fz}}{2}} J_{v_z-1}\left(a_n z_{wD}^{\frac{(2+\theta_z)}{2}}\right) - h_{wD}^{\frac{d_{fz}}{2}} J_{v_z-1}\left(a_n h_{wD}^{\frac{(2+\theta_z)}{2}}\right)\right\}}{a_n\left[J_{v_z-1}(a_n) - \frac{v_z}{a_n} J_{v_z}(a_n)\right]^2} \,. \tag{B.23}$$

Substituting Equation (A.7) into Equation (B.23), the final solution is given as follows:

$$\bar{p}_D(r_D, z_D, s) = \frac{2}{h_{pD} \cdot s} \cdot \sum_{n=0}^{\infty} \frac{r_D^{\frac{1-\beta_r}{2}} K_{v_r}\left[\left(\frac{2}{2+\theta_r}\right)\sqrt{s+\lambda_n} r_D^{\frac{2+\theta_r}{2}}\right] z_D^{\frac{1-\beta_z}{2}} J_{v_z}\left[a_n z_D^{\frac{2+\theta_z}{2}}\right]\left\{z_{wD}^{\frac{d_{fz}}{2}} J_{v_z-1}\left(a_n z_{wD}^{\frac{(2+\theta_z)}{2}}\right) - h_{wD}^{\frac{d_{fz}}{2}} J_{v_z-1}\left(a_n h_{wD}^{\frac{(2+\theta_z)}{2}}\right)\right\}}{\sqrt{s+\lambda_n}\left(\frac{1}{2}\right)\left[K_{v_r-1}\left[\left(\frac{2}{2+\theta_r}\right)\sqrt{s+\lambda_n}\right] + K_{v_r+1}\left[\left(\frac{2}{2+\theta_r}\right)\sqrt{s+\lambda_n}\right]\right] - \left(\frac{1-\beta_r}{2}\right) K_{v_r}\left[\left(\frac{2}{2+\theta_r}\right)\sqrt{s+\lambda_n}\right] a_n\left[J_{v_z-1}(a_n) - \frac{v_z}{a_n} J_{v_z}(a_n)\right]^2} \,, \tag{B.24}$$

where λ_n are the roots of Equation (B.10). The evaluation at the wellbore is obtained by evaluating Equation (B.24) for $r_D = 1$ in the producing interval, using:

$$\bar{p}_{wD}(s) = \frac{1}{h_{pD}} \int_{z_{wD}}^{h_{wD}} \bar{p}_{Df}(r_D = 1, z_D, s) dz_D \,. \tag{B.25}$$

Finally, the following expression is obtained for the wellbore pressure drop:

$$\bar{p}_{wD}(s) = \frac{2}{h_{pD}^2 \cdot s} \cdot \sum_{n=0}^{\infty} \frac{K_{v_r}[\psi_n]\left\{z_{wD}^{\frac{d_{fz}}{2}} J_{v_z-1}\left(a_n z_{wD}^{\frac{(2+\theta_z)}{2}}\right) - h_{wD}^{\frac{d_{fz}}{2}} J_{v_z-1}\left(a_n h_{wD}^{\frac{(2+\theta_z)}{2}}\right)\right\}^2}{\sqrt{s+\lambda_n}\left(\frac{1}{2}\right)\left[K_{v_r-1}[\psi_n] + K_{v_r+1}[\psi_n]\right] - \left(\frac{1-\beta_r}{2}\right) K_{v_r}[\psi_n] a_n^2\left[J_{v_z-1}(a_n) - \frac{v_z}{a_n} J_{v_z}(a_n)\right]^2} \,, \tag{B.26}$$

$$\psi_n = \left(\frac{2}{2+\theta_r}\right)\sqrt{s+\lambda_n} \,. \tag{B.27}$$

If Equation (B.26) is evaluated for $h_{pD} = 1$, $z_{wD} = 0$ and $h_{wD} = 1$, we obtain the fully penetrated well solution, given by:

$$\begin{aligned} \bar{p}_{wD}(s) = {} & \frac{K_{v_r}\left[\left(\frac{2}{2+\theta_r}\right)\sqrt{s}\right]}{s\left[\sqrt{s}\left(\frac{1}{2}\right)\left[K_{v_r-1}\left[\left(\frac{2}{2+\theta_r}\right)\sqrt{s}\right] + K_{v_r+1}\left[\left(\frac{2}{2+\theta_r}\right)\sqrt{s}\right]\right] - \left(\frac{1-\beta_r}{2}\right) K_{v_r}\left[\left(\frac{2}{2+\theta_r}\right)\sqrt{s}\right]\right]} \\ & + \frac{2}{h_{pD}^2 \cdot s} \cdot \sum_{n=1}^{\infty} \frac{K_{v_r}[\psi_n]\left\{z_{wD}^{\frac{d_{fz}}{2}} J_{v_z-1}\left(a_n z_{wD}^{\frac{(2+\theta_z)}{2}}\right) - h_{wD}^{\frac{d_{fz}}{2}} J_{v_z-1}\left(a_n h_{wD}^{\frac{(2+\theta_z)}{2}}\right)\right\}^2}{\sqrt{s+\lambda_n}\left(\frac{1}{2}\right)\left[K_{v_r-1}[\psi_n] + K_{v_r+1}[\psi_n]\right] - \left(\frac{1-\beta_r}{2}\right) K_{v_r}[\psi_n] a_n^2\left[J_{v_z-1}(a_n) - \frac{v_z}{a_n} J_{v_z}(a_n)\right]^2} \,. \end{aligned} \tag{B.28}$$

Thus, the pseudo-skin due to partial penetration considering fractal behavior is given by:

$$\bar{\xi}(s) = \frac{2}{h_{pD}^2 \cdot s} \cdot \sum_{n=1}^{\infty} \frac{K_{v_r}[\psi_n]\left\{z_{wD}^{\frac{d_{fz}}{2}} J_{v_z-1}\left(a_n z_{wD}^{\frac{(2+\theta_z)}{2}}\right) - h_{wD}^{\frac{d_{fz}}{2}} J_{v_z-1}\left(a_n h_{wD}^{\frac{(2+\theta_z)}{2}}\right)\right\}^2}{\sqrt{s+\lambda_n}\left(\frac{1}{2}\right)\left[K_{v_r-1}[\psi_n] + K_{v_r+1}[\psi_n]\right] - \left(\frac{1-\beta_r}{2}\right) K_{v_r}[\psi_n] a_n^2\left[J_{v_z-1}(a_n) - \frac{v_z}{a_n} J_{v_z}(a_n)\right]^2} \,. \tag{B.29}$$

References

1. Brons, F.; Martin, V.E. The Effect of Restricted Fluid Entry on Well Productivity. In Proceedings of the 34th SPE Annual Meeting, Dallas, TX, USA, 4–7 October 1959.

2. Gringarten, A.C.; Ramey Jr, H.J. An Approximate Infinite Conductivity Partially Penetrating Line-Source Solution Well. *SPE J.* **1975**, *15*, 140–148.
3. Bilhartz Jr, H.L.; Ramey Jr., H.J. The Combined Effect of Storage, Skin, and Partial Penetration on Well Test Analysis. In Proceedings of the SPE 52nd Annual Fall Technical Conference and Exhibition, Denver, CO, USA, 19–21 October 1977.
4. Yildiz, T.; Bassiouni, Z. Transient Pressure Analysis in Partially-Penetrating Wells. In Proceedings of the SPE International Technical Meeting, Calgary, AB, Canada, 10–13 June 1990.
5. Ozkan, E.; Raghavan, R. New Solutions for Well-Test-Analysis Problems: Part 1—Analytical Considerations. *SPE Form. Eval.* **1991**, *6*, 359–368.
6. Ozkan, E.; Raghavan, R. New Solutions for Well-Test-Analysis Problems: Part 2—Computational Considerations and Applications. *SPE Form. Eval.* **1991**, *6*, 369–378.
7. Bui, T.D.; Mamora, D.D.; Lee, W.J. Transient Pressure Analysis for Partially Penetrating Wells in Naturally Fractured Reservoirs. In Proceedings of the SPE Rocky Mountain Regional/Low Permeability Reservoirs Symposium and Exhibition, Denver, CO, USA, 12–15 March 2000.
8. Fuentes, G.; Camacho, R.; Vasquez, M. Pressure Transient and Decline Curve Behaviors for Partially Penetrating Wells Completed in Naturally Fractured-Vuggy Reservoirs. In Proceedings of the 2004 SPE International Petroleum Conference in Mexico, Puebla Pue., Mexico, 7–9 November 2004.
9. Miranda, F.; Barreto, A.; Peres, A. A Novel Uniform-Flux Solution based on Green's Functions for Modeling the Pressure Transient Behavior of a Restricted-Entry Well in Anisotropic Gas Reservoirs. *SPE J.* **2016**, *21*, 1–870.
10. Razminia, K.; Razminia, A.; Dastikhan, Z. A comprehensive Solution for Partially Penetrating Wells with Various Reservoir Structures. *J. Oil Gas Petrochem. Tech.* **2016**, *3*, 1.
11. Chang, J.; Yortsos, Y.C. Pressure Transient Analysis of Fractal Reservoirs. *SPE Form. Eval.* **1990**, *289*, 31.
12. Acuña, J.A.; Ershaghi, I.; Yortsos, Y.C. Practical Application of Fractal Pressure-Transient Analysis in Naturally Fractured Reservoirs. *SPE Form. Eval.* **1995**, *10*, 173–179.
13. Flamenco, L.F.; Camacho, R.G. Determination of Fractal Parameters of Fractured Networks Using Pressure-Transient Data. *SPE Reserv. Eval. Eng.* **2003**, *6*, 1.
14. Posadas, R.; Camacho, R.G.: Influence and determination of Mechanical Skin in a Reservoir with a Fractal Behavior. In Proceedings of the SPE Heavy and Extra Heavy Oil Conference, Lima, Peru, 19–20 October 2016.
15. Cossio, M.; Moridis, G.J.; Blasingame, T.A.: A Semianalytic Solution for Flow in Finite-Conductivity Vertical Fractures by Use of Fractal Theory. *SPE J.* **2013**, *18*, 83–96.
16. Wang, W.; Shahvali, M.; Su, Y. A semi-analytical fractal model for production from tight oil reservoirs with hydraulically fractured horizontal wells. *Fuel* **2015**, *158*, 612–618.
17. Wei, Y.; He, D.; Wang, J.; Qi, Y. A Coupled Model for Fractured Shale Reservoirs with Characteristics of Continuum Media and Fractal Geometry. In Proceedings of the SPE Asia Pacific Unconventional Resources Conference and Exhibition, Brisbane, Australia, 9–11 November 2015.
18. Raghavan, R.; Chen, C. Rate decline, power laws, and subdiffusion in fractured rocks. In Proceedings of the SPE Low Perm Symposium, Denver, CO, USA, 5–6 May 2016.
19. Fan, W.; Jiang, X.; Chen, S. Parameter estimation for the fractional fractal diffusion model based on its numerical solution. *Comput. Math. Appl.* **2016**, *71*, 642–651.
20. Xu, Y.; He, Z.; Agrawal, O.P. Numerical and analytical solutions of new generalized fractional diffusion equation. *Comput. Math. Appl.* **2013**, *66*, 2019–2029.
21. Raghavan, R.; Chen, C. Fractional diffusion in rocks produced by horizontal wells with multiple, transverse hydraulic fractures of finite conductivity. *J. Pet. Sci. Eng.* **2013**, *109*, 133–143.
22. Van Everdingen, A.F.; Hurst, W. The Application of Laplace Transformation to Flow Problems in Reservoirs. *Trans. AIME* **1949**, *180*, 305–324.
23. Stehfest, H. Numerical Inversion of Laplace Transforms. *Commun. ACM* **1970**, *13*, 47.
24. Lebedev, N.N. *Special Functions and Their Applications*; Prentice-Hall: Upper Saddle River, NJ, USA, 1965.
25. Abramowitz, M.; Stegun, I: *Handbook of Mathematical Functions*, Dover Publications: New York, NY, USA, 1965.
26. Gradshteyn, I.S.; Ryzhik, I.M. *Table of Integrals, Series, and Products*; Academic Press: Cambridge, MA, USA, 2007.

© 2019 by the authors. Licensee MDPI, Basel, Switzerland. This article is an open access article distributed under the terms and conditions of the Creative Commons Attribution (CC BY) license (http://creativecommons.org/licenses/by/4.0/).